

Computational prediction of electrical and thermal conductivities of disklike particulate composites

J. Qiu^{*,‡}, Y. B. Yi^{*,§} and X. Guo[†]

**Department of Mechanical and Materials Engineering
University of Denver
Denver, CO 80208, U.S.A*

*†Department of Electrical Engineering
University of Texas Dallas
Richardson, TX 75080, U.S.A*

‡Jian.Qiu@du.edu

§Yun-Bo.Yi@du.edu

Received 9 February 2015

Accepted 20 May 2015

Published 1 July 2015

The effective conductivities are determined for randomly oriented disklike particles using an efficient computational algorithm based on the finite element method. The pairwise intersection criteria of disks are developed using a set of vector operations. An element partition scheme has been implemented to connect the elements on different disks across the lines of intersection. The computed conductivity is expressed as a function of the disk density and size. It is further expressed in a power-law form with the key parameters determined from curve fitting. The particle number and the trial number of simulations vary with the disk size to minimize the computational effort in search of the percolation paths. The estimated percolation threshold agrees very well with the result reported in the literature. It has been confirmed that the statistical invariant for percolation is a cubic function of the characteristic size, and that the definition of percolation threshold is consistent with that of the equivalent system containing spherical particles. Binary dispersions of disks of different radii have also been investigated to study the effect of the size distribution. The approximate solutions in the power-law function have potential applications in advanced composites with embedded graphene nanoplatelets (GNPs).

Keywords: Multiscale modeling; disklike particle; Monte Carlo method; graphene nanoplatelets.

1. Introduction

Multiscale modeling of material properties of heterogeneous random composites has been an active research area for decades. Approximations using the effective medium theories (EMTs) are widely available in the literature [Kirkpatrick and Scott, 1973; Torquato, 2002], with examples including the rules of mixing [Wei *et al.*, 2004], the

[‡]Corresponding author.

Maxwell formula [Maxwell, 1881], the self-consistent approximation [Gubernatis and Krumhansl, 1975], and the differential EMT [McLaughlin, 1977]. However, there is always an uncertainty associated with the numerical accuracy of EMTs [Garboczi and Berryman, 1997]. In general, for those particulate materials with large aspect ratios, the Monte Carlo method has proved more efficient and accurate [Berhan *et al.*, 2009; Zhang and Yi, 2008]. For example, Kirkpatrick and Scott [1973] developed a predictive computational model using resistor networks in conjunction with the Monte Carlo simulation method. As a virtual experiment, such a model has the advantage of altering design parameters with a minimal cost. Some other pioneers in the area reported simulation results for the effects of various probabilistic or deterministic parameters in continuum percolation and conduction of spherical particles [Pike and Seager, 1974]. Other geometries, such as ellipsoids [Yi *et al.*, 2004], fibers and planar disks, were also modeled using the Monte Carlo scheme. For example, fibrous additions relevant to the battery technologies were examined for their conductive properties via modeling the material as a random fibrous network [Cheng and Sastry, 2004].

Despite these important achievements in the area, results were not reported until very recent for a special type of particulate materials, i.e., planar disks or plates oriented in the three-dimensional space. Disklike geometries are of particular interest because circular plates are the limiting cases of oblate ellipsoids of revolution when their thickness approaches zero. Recently the geometric percolation thresholds for plates of various shapes oriented in three dimensions were determined precisely by the Monte Carlo simulations [Yi and Tawerghi, 2009; Yi and Esmail, 2012]. The percolation points were estimated via linear or nonlinear extrapolations for circles, squares and equilateral triangles. These results showed that the noncircular shapes and corner angles in the plate geometry increase the probability of interparticle connectivity and therefore tend to reduce the percolation density. Compared to their ellipsoidal counterparts, plate-shaped particles can percolate at a much lower volume fraction and hence have potential applications in advanced composites wherein the main objective is to minimize the total amount of additions for achieving desirable material performances.

Disklike particles attracted special interest in the past decade, with a particular application related to graphene nanoplatelets (GNPs), which are disklike nanoparticles consisting of 10–100 layers of graphene produced through exfoliation. The diameters of these plates range from sub-micrometre to 100 micrometers [King *et al.*, 2013]. GNPs with an average thickness of 5–10 nanometres have unique mechanical and electrical properties due to their pure graphitic composition [Gao *et al.*, 2013]. In particular, both thermal and electrical conductivities can substantially be improved because graphene has two-dimensional lattice structure with extremely high aspect ratio. Furthermore, exfoliated graphene layers dispersed into materials that produce multiple conductive pathways in the composites also improve the conductivity [Stankovich *et al.*, 2006].

Due to these reasons graphene has been used in many advanced composites, such as electronic solder composites. It was found that graphene nanosheet doped to lead-free Sn–Zn–Bi solder alloys demonstrated higher conductivities and higher shear strength [Hu *et al.*, 2013]. In another experiment, it was found that with the increasing addition of graphene nanosheets, the nanocomposite solders showed an improvement in their wetting property and a decrease in the coefficient of thermal expansion [Liu *et al.*, 2013]. Furthermore, a decrease in ductility was recorded with the addition of graphene nanosheets. In some of the other applications, however, the property change can be a trade off that needs careful consideration. For example, a new design of power transmission line consists of aluminum conductor composite core (ACCC) [Alawar *et al.*, 2005; Burks *et al.*, 2010], in which the ECR-glass/epoxy layer is used to prevent a direct electrical path between the aluminum conducting wires in the periphery and the conductive carbon fibers in the core, thus preventing the galvanic reaction between them [Peng and Nie, 2013]. The current design of the insulating layer has shown a relatively weak mechanical stiffness and is vulnerable to external mechanical loads. A potential method to increase the mechanical stiffness of the ECR/epoxy layer is to add GNPs. However, the addition of the conductive graphene can raise the electrical conductivity in the composite and thus increase the probability of galvanic reaction. The overall addition of the conductive fiber contents should therefore be controlled below the percolation threshold to ensure that the barrier can still function as an electrical insulator.

To study the effect of the addition of disklike particles on the overall electrical conductivity of composite, the finite element method [Chen *et al.*, 2008; Garboczi and Day 1995], is a preferred method. An application of this method was explored by Roberts and Garboczi [2002] who studied material properties of random porous composites with various microstructures. However, reduction in local maximum errors, particularly at material boundaries, is not guaranteed in that method. In an alternative approach Cai *et al.* [2005] applied this concept to compute thermal conductivity of PTEE composite. In general, the finite element modeling of multiphase heterogeneous composites is by no means a routine task, since the fibrous or particulate inclusions are interconnected. The persistent obstacles to mesh automation of complex structures are well known and no individual commercial solver is capable of handling these difficulties [Tawerghi and Yi, 2009]. Development of a new, direct simulation method that does not rely on digitization of the material phase, thus allowing more accurate modeling of the interconnected structures, is therefore of great importance.

It should also be pointed out that despite the successful work on the percolation problems, a systematic study of the conductivity of randomly oriented disks is not widely available in the literature. In this study, an efficient computational algorithm for determining conductivities will be implemented. We will first establish an element partition scheme as well as a set of criteria for detecting interparticle connections followed by a finite element analysis. Then the curve fitting techniques

will be applied to estimate the percolation threshold along with the key parameters in the power-law approximations.

2. Methods

In this study, we assume a system of circular disks with negligible thickness uniformly distributed in a three-dimensional unit cell. Hence the centers of the disks are distributed with a constant probability density function, as shown in Fig. 1. The disks are fully penetrable and the orientation angles of the axis (i.e., the normals of disk planes) are also randomly distributed, following a particular probability density function [Yi and Sastry, 2004]. These disks form clusters and therefore the first necessary step in our modeling is to detect the pairwise connectivity of the disks.

2.1. Intersection criteria

Given two circular disks of radii r_1 and r_2 , by modifying the previously reported technique [Yi and Tawerghi, 2009], we developed the following intersection criteria in a more efficient way. We first determined the normal vectors \vec{n}_1 and \vec{n}_2 of the two disks based on their orientation angles. Assuming \vec{R} to be the position vector from the center of the second, we defined the following quantities:

$$\beta = \frac{\vec{R} \cdot \vec{n}_1}{\sqrt{1 - (\vec{n}_1 \cdot \vec{n}_2)^2}}; \tag{1}$$

$$a, b = \pm \sqrt{R_2^2 - \beta^2} + \frac{\vec{R} \cdot (\vec{n}_1 \times \vec{n}_2)}{\|\vec{n}_1 \cdot \vec{n}_2\|}; \tag{2}$$

$$c = \frac{\vec{R}_1 \cdot (\vec{n}_1 \times (\vec{n}_1 \times \vec{n}_2))}{\|\vec{n}_1 \times (\vec{n}_1 \times \vec{n}_2)\|} - \beta(\vec{n}_1 \cdot \vec{n}_2); \tag{3}$$

$$p = \sqrt{r_1^2 - c^2}. \tag{4}$$

It can be proved that the two disks intersect if and only if $r_2^2 - \beta^2 > 0$ and any of the following four conditions is satisfied:

- (i) $a^2 + y^2 \leq r_1^2$;
 - (ii) $b^2 + c^2 \leq r_1^2$;
 - (iii) $\|c\| < r_1$ & $(a - p)(b - p) < 0$;
 - (iv) $\|c\| < r_1$ & $(a + p)(a - p) < 0$.
- (5)

The above criteria have been validated by a computational realization of the random disks in Matlab, followed by an inspection of the actual interparticle connectivity. In the next step, we discretized the interconnected system to construct a continuous mesh for the subsequent finite element analyses.

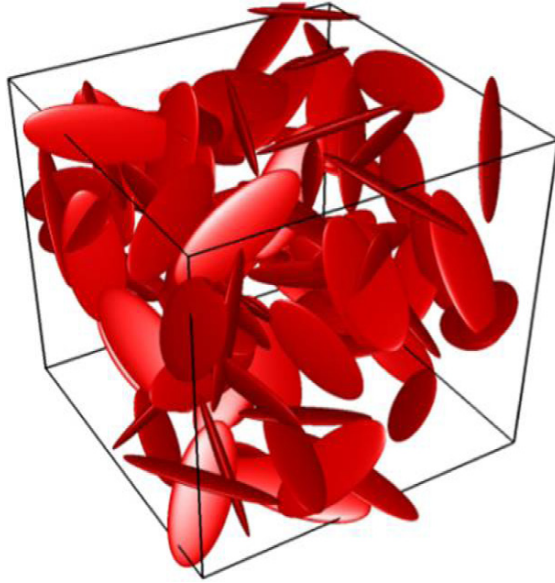


Fig. 1. A computational model showing a system of random circular disks.

2.2. Element generation and partition

The finite element analysis is the key step in the entire procedure to determine the equivalent conductivity of the disk system. In general, mesh generation is not a technically challenging problem, since numerous commercial finite element solvers are available in the market and these codes usually contain built-in automatic meshing algorithms. Their common strategy involves the description of the overall surface geometry. For example, a Boolean operation can be applied to a two-dimensional system of overlapping disks to obtain a union geometry. A finite element mesh can then be generated on the resulting geometry. A large, randomized heterogeneous system in three dimensions, however, requires meshing of a large number of particles in order to minimize the size effects in the subsequent analyses. For volume fractions exceeding the percolation threshold, it is generally difficult to describe the overall surface or volumetric geometries, without resorting to manual techniques.

In this study, we developed a new, automated mesh generation scheme. First, a triangular shell mesh was created on the surface of each individual disk using the mesh generation functionality embedded in COMSOL[®] [COMSOL USERS MANUAL, 2006, Version 3.3, COSMOL, Inc. USA]. The local mesh density is curvature dependent, therefore a few parameters including the curvature cutoff threshold and maximum element size were defined to avoid excessive local elements and numerical inaccuracy induced by the local singularities of the solution. The elements were then translated and rotated to the locations specified. These triangular elements were later used as a basis to create interfacial elements. The disk size was fixed

throughout and the changing of disk density was made by varying the disk number. The thickness of disk was assumed to be much smaller than the diameter, and therefore no discretization was performed along the thickness direction.

When two disks meet, the two planes form a line of intersection. A standard finite element analysis requires continuous connections of elements at the boundaries. To connect the elements located on the two different planes, a partition scheme was implemented to cut the triangular elements across the line of intersection. A strategy was introduced in the scheme in which we first determined the spatial locations of the intersection points formed by the edges of one triangle and the plane formed by the other triangle, as shown in Fig. 2. The line of intersection between the two planes was then obtained by connecting the two intersection points. In Fig. 2, the location of the intersection point F of a line DE and the plane defined by the triangle ABC was determined from the following vector operations,

$$\vec{FD} = \vec{DE} \left(\frac{|DG|}{|DH|} \right) = \vec{DE} \left(\frac{\vec{AD} \cdot \vec{n}}{\vec{ED} \cdot \vec{n}} \right), \tag{6}$$

where

$$\vec{n} = \frac{\vec{AB} \times \vec{AC}}{|\vec{AB} \times \vec{AC}|} \tag{7}$$

and

$$\vec{r}_F = \vec{r}_D - \vec{FD} = \vec{r}_D - \vec{DE} \left(\frac{\vec{AD} \cdot \vec{n}}{\vec{ED} \cdot \vec{n}} \right). \tag{8}$$

This method allows for determination of the two intersection points, whose positions relative to the triangle could be categorized into the following cases:

- (i) located at vertex of the triangle;
- (ii) located along an edge of the triangle;

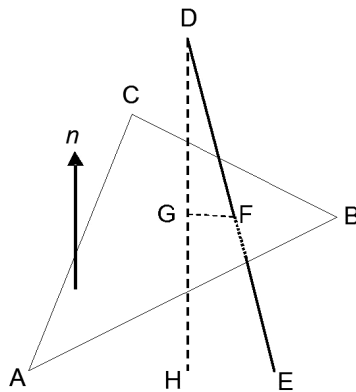


Fig. 2. A Schematic showing the determination of the location of intersection point between a line and a plane formed by a triangle.

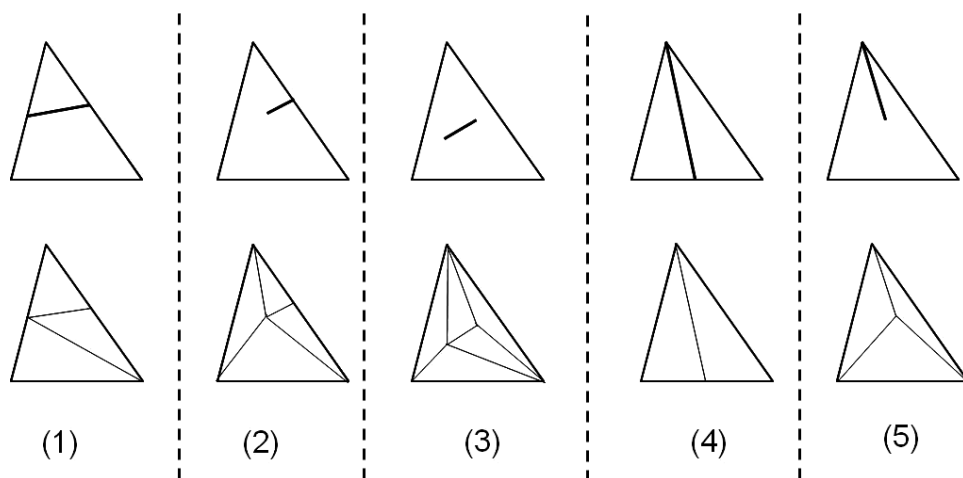


Fig. 3. Five possible configurations involved in the element partition schemes, with the top row representing the different locations of the line of intersection and the bottom row representing the new elements created by the scheme.

- (iii) located in the interior of the triangle;
- (iv) located in the exterior of the triangle.

Depending on the locations of the intersection points, an element can be partitioned into multiple smaller elements. From a close inspection of all possible scenarios, we have found that there exist only six distinct configurations that should be treated separately, as illustrated in Fig. 3. It turns out that the minimum number of the new elements is two when one of the intersection points is located at a vertex and the other is located on an edge (i.e., case #4); whereas the maximum number of the new elements is five when both points are located in the interior of the triangle (i.e., case #3).

Figure 4 shows an example in which two adjacent triangles have been partitioned by a line of intersection. The elements shown on the left and the right represent the configurations before and after the partition was applied, respectively. Multiple results are possible in each case. For example, the triangle on the left in Fig. 4(a) can actually be divided into four or more new triangles, rather than three as shown

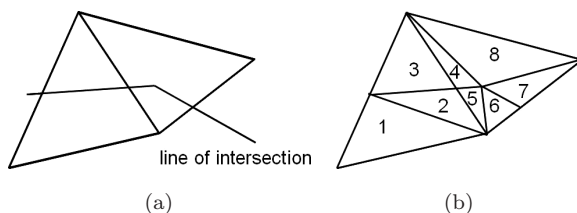


Fig. 4. An example showing two adjacent triangular elements: (a) Before partition; (b) after partition.

in Fig. 4(b). Overall, our objective is to minimize the number of the newly created nodes and elements. In some cases, it is necessary to locate the intersection of two line segments on a same plane. Suppose AB and CD are two arbitrary line segments located on the same plane. The location of an arbitrary point $r(x, y, z)$ on either of the two lines can be expressed as:

$$\begin{aligned} r &= r_A + (r_B - r_A)t, \\ r &= r_C + (r_D - r_C)s, \end{aligned} \tag{9}$$

where both t and s are the local coordinates ranging between 0 and 1. By solving the simultaneous equations for x and y , we have:

$$\begin{aligned} s &= \frac{(x_A - x_C)(y_B - y_A) - (y_A - y_C)(x_B - x_A)}{(x_A - x_B)(y_D - y_C) - (y_A - y_B)(x_D - x_C)}, \\ t &= \frac{(x_A - x_C)(y_D - y_C) - (y_A - y_C)(x_D - x_C)}{(x_A - x_B)(y_D - y_C) - (y_A - y_B)(x_D - x_C)}. \end{aligned} \tag{10}$$

When the two lines intersect, there must be a unique solution to the above equations. To ensure the existence of such a solution, the denominator must be nonzero, leading to

$$\Delta = |(x_A - x_B)(y_D - y_C) - (y_A - y_B)(x_D - x_C)|. \tag{11}$$

Figure 5 shows a couple of examples of the element mesh formed by three intersecting disks after the partitions scheme was applied. It can be seen that the continuity is satisfied at the interfaces of the disk planes. For a realistic system containing a large number of disks, the pairwise connections among the disks were examined and the element partition scheme was applied whenever such a connection was detected. A complete finite element model containing 1000 disks of radius 0.07 and approximately 100,000 elements is shown in Fig. 6, using this automated mesh generation scheme.

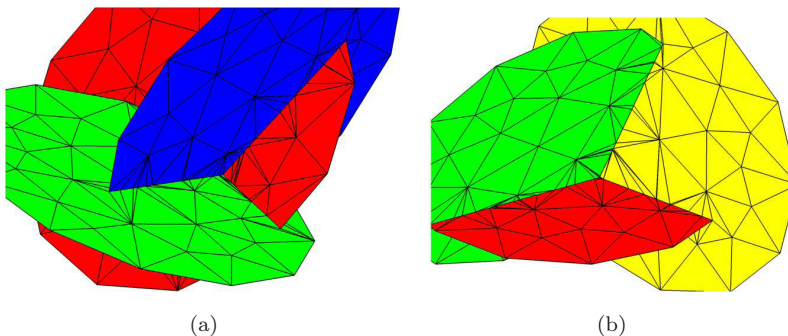


Fig. 5. Example showing the finite elements created for a cluster of three disks with the successful implementation of the element partition scheme.

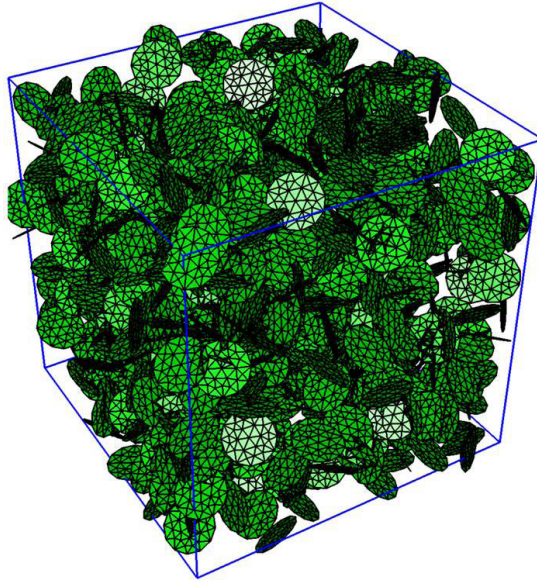


Fig. 6. A complete finite element mesh for the entire model with 1000 disks of radius 0.07 and approximately 100,000 elements.

2.3. Finite element analysis

The mesh data including the nodal positions and element compositions were exported to an ABAQUS [ABAQUS STANDARD USERS MANUAL, 2009, Version 6.9, Dassault Systems Simulia Corp.; USA] script file. The effective conductivity of the material system was computed from a steady state heat conduction analysis. More specifically, a DS3 element type (namely, three-node triangular shell element for thermal analysis) was selected. The kinetic degrees of freedom were absent and the temperature was the only remaining degree of freedom in the analysis. A unit temperature difference was specified on the two opposite sides of the unit cell and the reactive heat flux was computed. Thermal conduction took place due to the temperature gradient and the steady state solution was sought by solving Laplace's equation. It can be proved that the total flow rate by summing the nodal heat flux is equivalent to the effective conductivity of the system. Despite the physical distinction between thermal and electrical conductions, the normalized computational result here can be interpreted as either the thermal conductivity or the electrical conductivity because of the mathematical and physical analogies between the two phenomena.

We varied the disk radius from 0.05 to 0.15 in our simulations. The smallest disk size corresponds to one tenth of the unit cell and the largest size is approximately one third of the unit cell. In the former case the boundary effect is negligible whereas in the latter case the boundary imposes a significant constraint to the system. Therefore we were able to study the scaling effect on the simulation results. The

simulations were run for 10–20 times at each volume fraction (or equivalently, each number of disks) depending on the disk radius. The results were collected and the means and the standard deviations were computed afterwards.

2.4. Percolation threshold

Theoretically percolation occurs at the transition of conductivity from zero to a nonzero value for an infinite system. In the simulations, the exact location of this transition is highly probabilistic due to the finite size effect and the percolation threshold can be estimated from a statistical analysis of the results. The percolation threshold can generally be expressed in terms of either the area fraction for two-dimensional particles or the volume fraction for three-dimensional particles. In the present study the disklike geometries are two-dimensional but they are oriented in space. We hypothesize that the statistical invariant for disks in three dimensions follows a cubic function of the characteristic length and that the definition of percolation threshold is consistent with its spherical counterpart. We define the following quantity to measure the percolation threshold:

$$\eta = \frac{4}{3}N\pi r^3, \quad (12)$$

where r is the disk radius and N is the total disk number. As r approaches zero, N would become infinite for percolation, meanwhile η would become an invariant η_c . Therefore η can be interpreted as the normalized disk size and will be used throughout our discussion in the remaining sections. We will later verify this hypothesis through simulations.

3. Results

3.1. Effect of disk thickness

There are a few parameters that can affect the conducive performance of material: (1) The diameter of disks; (2) the total number of disks; (3) the disk thickness; (4) the conductivity of the disk material; (5) the distributions of the parameters (including size, center location and orientation angles). To simplify the problem we assume uniform distributions of the locations and orientation angles and therefore the last factor is not taken into consideration here in our study.

We first investigated the effect of disk thickness on the conductivity using a pair of fixed parameters $r = 0.07$ and $N = 1000$. We varied the disk thickness from 0.001 to 0.01 by modifying the solid section definitions of the sell elements in the finite element analysis. From the elemental theory of electrical or heat conduction, a greater size of the cross section allows for a higher rate of conduction. Therefore the conductivity must be proportional to the cross sectional area, and hence the thickness. This has been confirmed in Fig. 7, which shows the conductivity as a strictly linear function of the disk thickness. Due to this reason, in the following

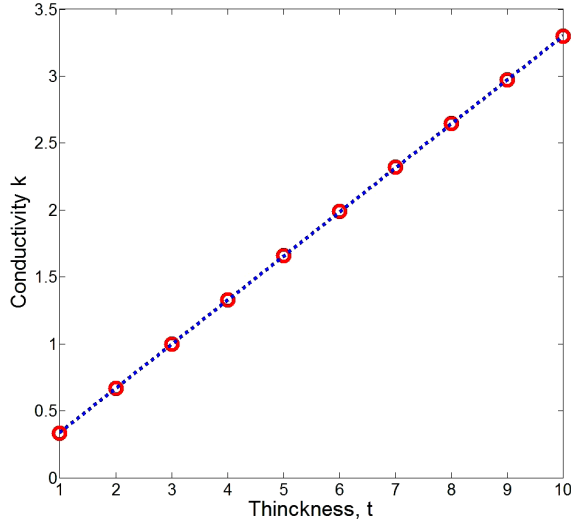


Fig. 7. Conductivity as a function of disk thickness.

discussion we define a dimensionless conductivity K that is normalized against the disk thickness, which is defined as:

$$K = \frac{K_{\text{eqv}}}{K_{\text{disk}}h}, \quad (13)$$

where K_{eqv} represents the computed conductivity of the entire system, K_{disk} is the conductivity of the disk material, and h represents the disk thickness. In this way we believe that the simulation results can be presented clearly and succinctly.

3.2. Power-law fitting of conductivity

Shown in Fig. 8 are the simulation results of the equivalent conductivity expressed as a function of the disk number for four different radii ranging from 0.05 to 0.15. The total number of disks varies from 1800 to 70 accordingly. To evaluate the statistical variations, the simulations were repeated 10 or 20 times for each radius, with larger radii requiring more simulation trials. Apparently the conductivity remains zero when insufficient number of disks is incorporated to form conductive pathways in the system. The result becomes nonzero as the disk number reaches a critical value that is equivalent to the percolation threshold. Beyond this critical value the conductivity increases nonlinearly. This is consistent with the results reported in the literature for heterogeneous materials containing inclusions of other geometrical shapes. In addition it is shown in the figure that fewer disks are present in the model when the disk size increases, resulting in a greater variation. The simulation results can approximately be fitted into a power-law form using the least-squares scheme:

$$K = A(N - N_0)^t, \quad N > N_0. \quad (14)$$

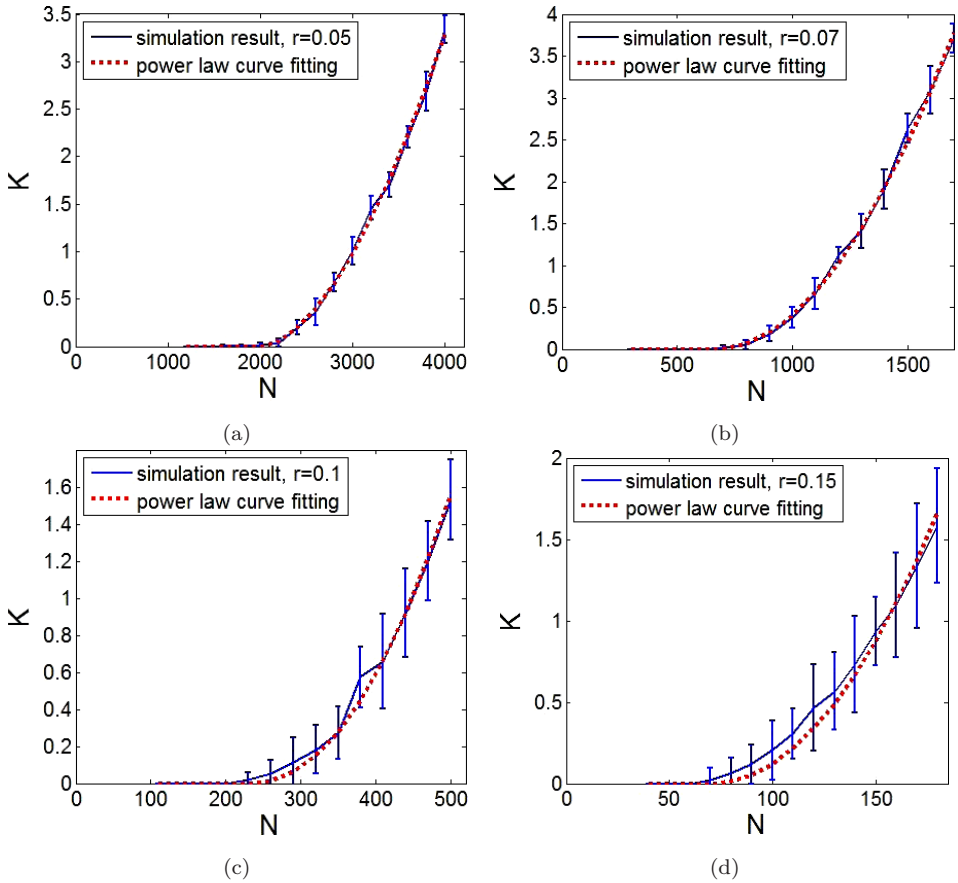


Fig. 8. Conductivity as a function of disk number for four different radii $r = 0.05, 0.07, 0.1$ and 0.15 .

Table 1. Power-law curve fitting results based on Eq. (14).

Radius, r	A	N	t	Squared norm residual
0.05	7.2177×10^{-7}	1838.014	2.0000	1.8351×10^{-6}
0.07	5.1105×10^{-6}	673.199	1.9488	3.2237×10^{-6}
0.10	1.1106×10^{-5}	230.152	2.1177	6.2008×10^{-6}
0.15	1.3246×10^{-4}	70.001	2.0082	1.4871×10^{-5}

Matlab function *lsqcurvefit* has been used in curve fitting and the estimated coefficients A , N_0 and t are presented in Table 1 along with the estimated errors. Apparently N_0 is not a constant since more disks are required to reach percolation as the disk size is reduced. The exponent, t , however, is approximately a constant with an average value around 2.02.

Since the critical disk number N_0 is not an invariant, it is preferable to use the quantity η as defined previously in place of N in the approximate formula. Figures

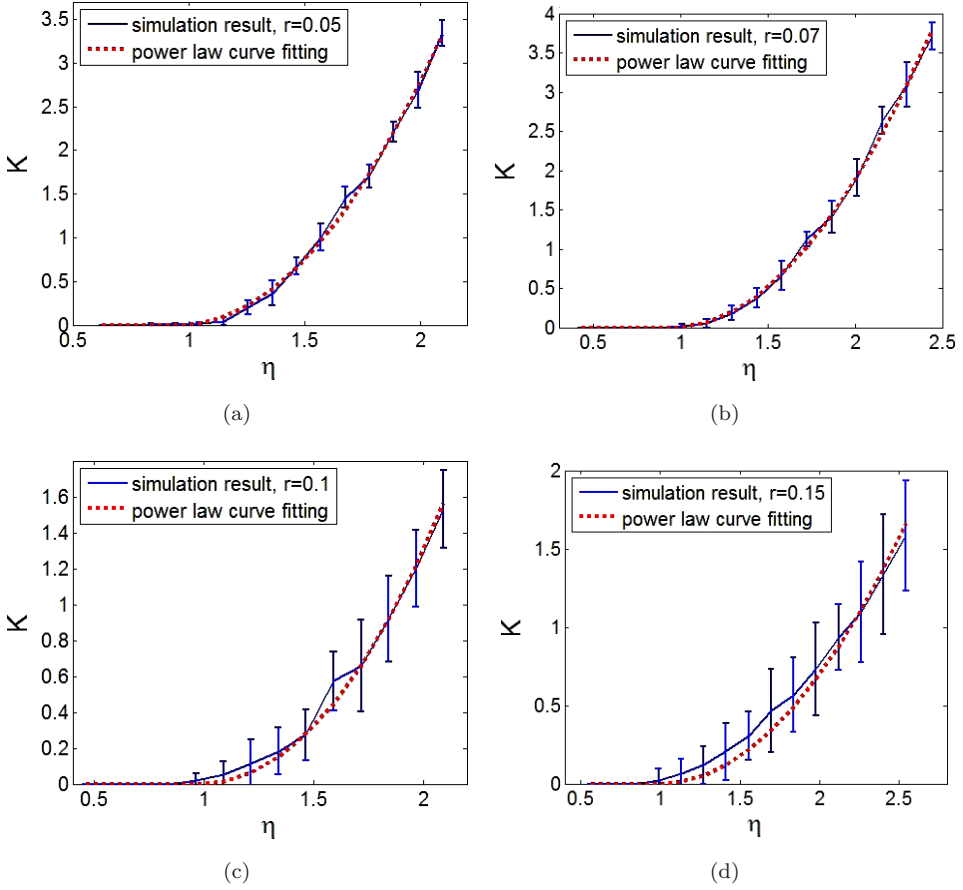


Fig. 9. Conductivity as function of η defined in Eq. (12) for four different radii $r = 0.05, 0.07, 0.1$ and 0.15 .

9(a)–9(d) show the conductivity as a function of η for four different disk radii $0.05, 0.07, 0.1$, and 0.15 , respectively. The power law function should then be expressed in the modified form as follows:

$$K = \sigma_0(\eta - \eta_0)^t, \quad \eta > \eta_0 \tag{15}$$

with the parameters tabulated in Table 2. The conductivity rapidly increases as η exceeds η_0 . The same figures also show that the variation in the result increases with the radius. In fact the average standard deviation increases from 8.47×10^{-5} at $r = 0.05$ to 2.01×10^{-4} at $r = 0.15$, due to the reduced disk number for percolation.

3.3. Estimation of percolation threshold

As r approaches zero, N_0 approaches infinity for percolation. However, according to the percolation theory, η_0 approaches a constant value, which is defined as the

Table 2. Power-law curve fitting results based on Eq. (15).

Radius, r	σ_0	η_0	t	Squared norm residual
0.05	2.596	0.9624	2.0000	8.4668×10^{-5}
0.07	1.771	0.9672	1.9488	1.9488×10^{-4}
0.10	1.206	0.9641	2.1177	2.1177×10^{-4}
0.15	0.687	0.9896	2.0082	2.0082×10^{-4}

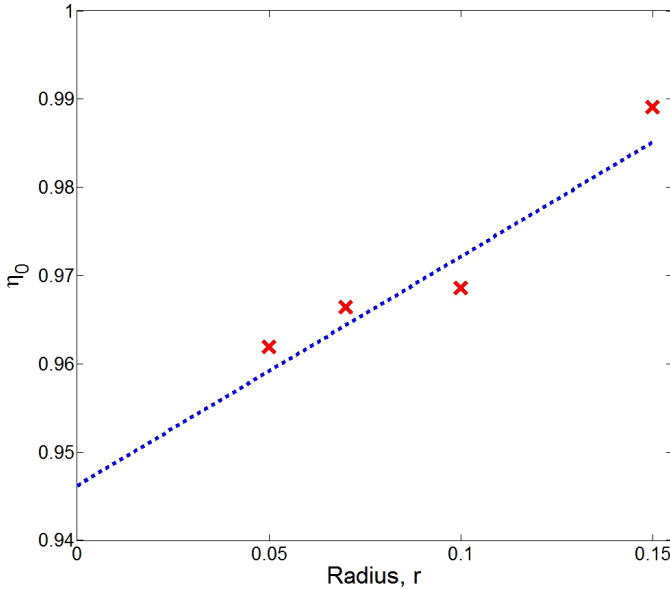


Fig. 10. Determination of percolation threshold at $r = 0$ using linear extrapolation.

percolation threshold of the system, η_c . We have observed a slight increase in η_0 as r increases. To estimate the percolation threshold we applied a linear extrapolation to find the intersection of η_0 at $r = 0$, as shown in Fig. 10. Based on the curve fitting, we estimated a solution of $\eta_c = 0.9462 \pm 0.0001$. This value of η_c is slightly lower than the solution reported previously, which is $\eta_c = 0.9614 \pm 0.0006$, with a difference around 1.6% [Yi and Tawerghi, 2009]. The underestimated result in the current study could be related to the finite element analysis, which is an approximate method, as well as the different number of disks used in the two distinct models. It should be noted that the previous study in the literature involved the detection of percolation paths based on geometric connectivity without using numerical approximations. Therefore it is not surprising to see the discrepancy in the two solutions. Nevertheless it is a good agreement in view of the order of magnitude in the error. Generally speaking the solution obtained from the finite element analysis is less accurate since the matrix operations required in the finite element analysis cost substantially more computational effort.

By applying a similar technique, we successfully obtained an approximate value $\sigma \approx 4.64$ as r approaches zero. However, a logarithm function was used in the curve fitting due to the high nonlinearity in the relationship between r and σ_0 . Therefore in the limiting case, the power-law function can be written in the following approximate form:

$$K = 4.64(\eta - 0.946)^{2.02}, \quad r \rightarrow 0. \tag{16}$$

3.4. Binary mixture of disks of different sizes

We also investigated the effect of the size distribution on the conductivity by introducing a binary sized distribution of disks of two different radii, r_1 and r_2 , as shown in Fig. 11. We define the ratio of the two radii to be $\lambda = r_1/r_2$. Assume the two types of disks have the same number and we have $f = 0.5$ where f represents the fraction of disks of radius r_1 . We fixed the total disk number in this binary distribution while chose the value of r such that the corresponding η defined in Eq. (12) is maintained the same as that of the equisized disk system. If the equisized disks have radius r , then the relationship between r and r_1, r_2 can be found as:

$$2r^3 = r_1^3 + r_2^3 \tag{17}$$

and thus

$$r_2 = r \left(\frac{2}{1 + \lambda^3} \right)^{1/3}, \quad r_1 = \lambda r_2. \tag{18}$$

Based on these assumptions, simulations can be performed in a fashion similar to the equisized disk system and the resulting percolation threshold, η_c can be evaluated

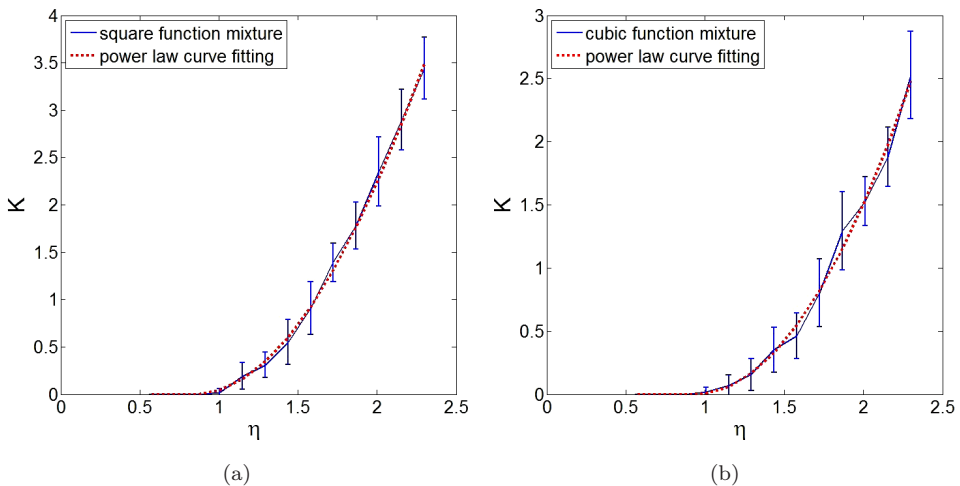


Fig. 11. A comparison of conductivity between two different types of binary mixture of disks, using (a) the square function equivalence; (b) the cubic function equivalence.

Table 3. Power-law curve fitting results for a binary mixture of disks of two different radii.

Type of mixing	σ_0	η_0	t	Squared norm residual
Cubic function	1.346	0.9407	2.0027	5.7716×10^{-6}
Square function	1.749	0.8616	1.9150	4.6736×10^{-6}

as well. We set $\lambda = 2$ and $r = 0.07$, therefore,

$$r_1 = 0.08480, \quad r_2 = 0.04240. \tag{19}$$

In addition to this work, we also investigated a binary mixture using the equivalent area instead of volume. This is driven by the fact that each individual disk is a two dimensional geometry. To do so, we considered

$$2r^2 = r_1^2 + r_2^2. \tag{20}$$

Setting $\lambda = 2$ and $r = 0.07$ leads to

$$r_1 = 0.08854, \quad r_2 = 0.04427. \tag{21}$$

Table 3 shows the simulation results of percolation threshold for the two different types of binary mixture of disks. It has been found that $\eta_c = 0.9407$ for the case using the cubic function, and $\eta_c = 0.8616$ for the case using the square function. Compared to the result from the uniform dispersion, apparently the cubic function yields a much closer solution with a difference only about 0.6%. It is again confirmed that the statistical invariant for percolation of disks must be a cubic function of the characteristic length. The result also implies that one can use the average particle size in a polydisperse system to approximate the equivalent conductivity with a reasonably good accuracy if the variation in the particle size is not quite significant (e.g., when $0.5 < \lambda < 2$).

4. Conclusion

The effective conductivities of randomly positioned and oriented circular plates are determined using an efficient computational algorithm based on the Monte Carlo modeling and the finite element method. The disks are discretized using a specialized element partition scheme to construct a continuous mesh that consists of interconnected shell elements. The equivalent conductivity is computed from the reactive flux in a simulation cell subjected to a unit potential across the domain. The computational algorithms are optimized to accommodate particles of different sizes and to minimize the computational time. It has been found that the results can be fitted into a power-law function and the key parameters in the function have been determined from the curve fitting techniques. The estimated percolation threshold is in the close vicinity of the prior results reported in the literature, where a different solution method was used. It has also been confirmed that the definition of percolation threshold is consistent with that of the equivalent particulate system

in three dimensions. For a binary sized distribution of disks with half of the disks having radii twice as large as the others, it has been found that the concept using the equivalent volume yields more accurate results compared to the equivalent area, and therefore the statistical invariant is indeed a cubic function of the characteristic size of the system. Due to the analogy between electrical and thermal conductions, the dimensionless results reported here can be interpreted as either electrical conductivity or thermal conductivity. The methods and results in this study are useful in predicting conduction and percolation of both monodisperse and polydisperse materials that contain disklike particles, and have potential applications in predicting the material properties of graphene platelets. The limitation of the current study lies in the assumption that the disks are fully overlapping. Future studies will involve partially penetrable disks that reflect more realistic conditions.

Acknowledgment

The authors would like to acknowledge support from the National Science Foundation under contract number #1232520.

References

- Alawar, A., Boseze, E. J. and Nutt, S. R. [2005] "A composite core conductor for low sag at high temperatures," *IEEE Trans. Power Delivery* **20**(3), 2193–2199.
- Berhan, L., Yi, Y. B., Sastry, A. M., Munoz, E., Selvidge, M. and Baughman, R. [2009] "Mechanical properties of nanotube sheets: Alterations in joint morphology and achievable moduli in manufacturable materials," *J. Appl. Phys.* **95**(8), 4335–4345.
- Burks, B., Armentrout, D. L. and Kumosa, M. [2010] "Failure prediction analysis of an ACCC conductor subjected to thermal and mechanical stresses," *IEEE Trans. Dielectrics Electr. Insulation* **17**(2), 588–596.
- Cai, W. Z., Tu, S. T. and Tao, G. L. [2005] "Thermal conductivity of PTFE composites with three-dimensional randomly distributed fillers," *J. Thermoplastic Composite Mater.* **18**(3), 241–253.
- Cheng, X. and Sastry, A. M. [2004] "On transport in stochastic, heterogeneous fibrous domains," *Mech. Mater.* **31**(12), 765–786.
- Chen, J., Xu, L. and Li, H. [2008] "Investigation on a direct modeling strategy for the effective elastic moduli prediction of composite material," *Mater. Sci. Eng. A* **491**(1), 385–389.
- Gao, J., Hu, M., Dong, Y. and Li, R. K. [2013] "Graphite–nanoplatelet decorated polymer with improved thermal, electrical, and mechanical properties," *ACS Appl. Mater. Interfaces* **5**(16), 7758–7764.
- Garboczi, E. J. and Berryman, J. G. [1997] "Elastic moduli of a materials containing composite inclusions: Effective medium theory and finite element computations," *Mech. Mater.* **33**(8), 445–470.
- Garboczi, E. J. and Day, A. R. [1995] "An algorithm for computing the effective linear elastic properties of heterogeneous materials: Three-dimensional results for composites with equal phase Poisson ratios," *J. Mech. Phys. Solids* **43**(9), 1349–1362.
- Gubernatis, J. E. and Krumhansl, J. A. [1975] "Macroscopic engineering properties of polycrystalline materials: Elastic properties," *J. Appl. Phys.* **46**(5), 1875–1883.

- Hu, X., Chan, Y. C., Zhang, K. and Yung, K. C. [2013] "Effect of graphene doping on microstructural and mechanical properties of Sn8Zn3Bi solder joints together with electromigration analysis," *J. Alloys Compound* **580**(6), 162–171.
- King, J. A., Klimek, D. R., Miskioglu, I. and Odegard, G. M. [2013] "Mechanical properties of graphene nanoplatelet/epoxy composites," *J. Appl. Polym. Sci.* **128**(6), 4217–4223.
- Kirkpatrick, S. [1973] "Percolation and conduction," *Rev. Modern Phys.* **45**(4), 574.
- Liu, X. D., Han, Y. D., Jing, H. Y., Wei, J. and Xu, L. Y. [2013] "Effect of graphene nanosheets reinforcement on the performance of Sn Ag Cu lead-free solder," *Mater. Sci. Eng. A* **562**(1), 25–32.
- Maxwell, J. C. [1881] *A treatise on electricity and magnetism* (Charendon press).
- McLaughlin, R. [1977] "A study of the differential scheme for composite materials," *Int. J. Eng. Sci.* **15**(4), 237–244.
- Peng, Z. and Nie, X. [2013] "Galvanic corrosion property of contacts between carbon fiber cloth materials and typical metal alloys in an aggressive environment," *Surface Coating Technol.* **21**(5), 85–89.
- Pike, G. B. and Seager, C. H. [1974] "Percolation and conductivity: A computer study.I," *Phys. Rev. B* **10**(4), 1421.
- Roberts, A. P. and Garboczi, E. J. [2002] "Computation of the linear elastic properties of random porous materials with a wide variety of microstructure," *Proc. R. Soc. Lond. A* **458** (2001) 1033–1054.
- Stankovich, S., Dikin, D. A., Dommett, G. H., Kohlhaas, K. M., Zimney, E. J., Stach, E. A. and Ruoff, R. S. [2006] "Graphene-based composite materials," *Nature* **442**(7100), 282–286.
- Tawerghi, E. and Yi, Y. B. [2009] "A computational study on the effective properties of heterogeneous random media containing particulate inclusions," *J. Phys. D: Appl. Phys.* **42**(17), 175409.
- Torquato, S. [2002] *Random Heterogeneous Materials: Microstructure and Macroscopic Properties* (Springer Science & Business Media, Inc., New York).
- Wei, C., Srivastava, D. and Cho, K. [2004] "Centrifuge testing," *Nano Lett.* **4**(10), 1949–1952.
- Yi, Y. B. and Esmail, K. [2012] "Computational measurement of void percolation thresholds of oblate particles and thin plate composites," *J. Appl. Phys.* **111**(12), 124903.
- Yi, Y. B. and Sastry, A. M. [2009] "Analytical approximation of the percolation threshold for overlapping ellipsoids of revolution," *Proc. Roy. Soc. Lond. Ser. A: Math., Phys. Eng. Sci.* **460**(2), 2353–2380.
- Yi, Y. B. and Tawerghi, E. [2009] "Geometric percolation threshold of interpenetrating plates in three-dimensional space," *Phys. Rev. E* **79**(4), 041134.
- Yi, Y. B., Wang, C. W. and Sastry, A. M. [2004] "Two-dimensional vs. three-dimensional clustering and percolation in fields of overlapping ellipsoids," *J. Electrochem. Soc.* **158**(8), A1292–A1300.
- Zhang, T. and Yi, Y. B. [2008] "Monte Carlo simulations of effective electrical conductivity in short-fiber composites," *J. Appl. Phys.* **103**(1), 014910.